

In-depth understanding of π -electron systems: New vistas in fullerene endohedrals*

Michio Yamada¹, Takahiro Tsuchiya¹, Takeshi Akasaka^{1,‡}, and
Shigeru Nagase²

¹Center for Tsukuba Advanced Research Alliance, University of Tsukuba, Tsukuba, Ibaraki 305-8577, Japan; ²Department of Theoretical and Computational Molecular Science, Institute for Molecular Science, Myodaiji, Okazaki 444-8585, Japan

Abstract: The synthesis and characterization of various endohedral metallofullerenes and their derivatives are described. The encapsulated metal atoms' positions and movements were determined using NMR study, X-ray crystallographic analysis, and theoretical calculations. The results of electrochemical investigations clarified the relation between the electronic properties and the π -electron systems of the fullerene endohedrals.

Keywords: endohedral fullerenes; fullerenes; metallofullerenes; π -electron systems; paramagnetic shift.

INTRODUCTION

Since the discovery of the fullerene in 1985 [1], numerous studies have been conducted to conceptualize and develop future applications of that new type of carbon material. Atom doping is a powerful methodology to modulate electronic properties in the field of materials science. Regarding fullerenes, endohedral atom doping provides novel carbon materials possessing fascinating properties. In particular, endohedral metal doping produces hybrid molecules of a new class: so-called endohedral metallofullerenes [2,3]. These days, endohedral metallofullerenes have attracted wide interest as spherical molecules with novel properties that are wholly unexpected in hollow fullerenes such as C₆₀. Because of the electron transfer from the encapsulated metal atoms to the fullerene cage, the metal atoms are cationic; the fullerene sphere itself is negatively charged. Therefore, the determination of the metal atoms' positions and movements is a crucial issue to clarify the physical and chemical properties of endohedral metallofullerenes. However, the structures and the metal positions or movements, in addition to their electronic properties, have remained obscured by the much lower yields of these species.

Recently, we developed a method of high-yield synthesis of endohedral metallofullerenes. To unveil their fascinating structures and properties, we systematically synthesized and characterized a series of endohedral metallofullerenes with various carbon cages and quantities of metals [4]. In particular, we examined Ce metallofullerenes. The existence of an f-electron spin on the Ce atom enables us to examine the paramagnetic effects to reveal the encapsulated metal atom's positions and movements. Furthermore, chemical derivatization was conducted to investigate the effects resulting from exohedral functionalization. Throughout this paper, we will provide some insights for evaluating and controlling

*Pure Appl. Chem. **82**, 757–1063 (2010). An issue of reviews and research papers based on lectures presented at the 13th International Symposium on Novel Aromatic Compounds (ISNA-13), 19–24 July 2009, Luxembourg City, Luxembourg on the theme of aromaticity.

‡Corresponding author: E-mail: akasaka@tara.tsukuba.ac.jp; Fax: (+81) 29-853-6409

the positions and movements of untouchable metal atoms inside spherical π -spaces, along with some insights into their electronic properties.

EXPERIMENTAL

Endohedral metallofullerenes are synthesized in a modified Krätschmer–Huffman generator. A composite rod containing graphite and metal oxide was subjected to an arc discharge as an anode. After annealing, the rod was vaporized in a helium atmosphere by arc discharge. We optimized the arc-discharge conditions (arc current = 256 A, arc voltage = 35 V, and He pressure = 150 Torr) to improve the yields. Carbonaceous soot containing empty fullerenes and endohedral metallofullerenes was obtained. From among the components, soluble fullerene species were extracted from the soot by refluxing in an organic solvent such as *N,N*-dimethylformamide (DMF). Then the extracts were subjected to high-performance liquid chromatography (HPLC) to isolate endohedral metallofullerenes.

RESULTS AND DISCUSSION

Molecular structure of Ce@C_{2v}-C₈₂

Actually, M@C_{2v}-C₈₂S [5] (M = group 3 metals and lanthanides) are readily available as the most abundant endohedral species using general arc discharge method. Because three valence electrons were transferred from the metal atom to the cage, the resulting open-shell electronic structure is described formally as M³⁺(C_{2v}-C₈₂)³⁻. Their paramagnetic nature has prevented us from performing NMR spectroscopic studies of them. In this context, one-electron reduction of the paramagnetic metallofullerenes has enabled the ¹³C NMR study of their anions to elucidate their cage structures [6–10]. However, the metal position in C_{2v}-C₈₂ cage has remained controversial [11–15]. To clarify the metal position, we performed paramagnetic NMR shift analyses of Ce@C_{2v}-C₈₂ anion [16].

First, the bond connectivity in Ce@C_{2v}-C₈₂ anion was determined and all the ¹³C NMR signals were fully assigned using 2D incredible natural abundance double-quantum transfer experiment (INADEQUATE) NMR study. This complete assignment enabled us to carry out the following paramagnetic NMR shift analyses. Because the f-electron spin on the Ce atom interacts with nucleus spins on the cage carbons, all carbon chemical shifts (δ) of the cage carbons show considerable temperature dependence. The chemical shifts of paramagnetic molecules in solution are generally expressed as a sum of three contributions from diamagnetic (δ_{dia}), Fermi contact (δ_{fc}), and pseudocontact (δ_{pc}) shifts, in which the paramagnetic δ_{fc} and δ_{pc} are proportional to T^{-1} and T^{-2} (T = absolute temperature), respectively (eq. 1) [17]. Constants c_{fc} and c_{pc} signify characteristic values of individual carbon signals. The δ_{dia} values correspond to the chemical shifts of the diamagnetic La@C_{2v}-C₈₂ anion [18]. In our case, the anisotropic pseudocontact interaction makes a more dominant contribution than the isotropic Fermi contact interaction because no meaningful connection exists between the Ce atom and cage carbons. This consideration was confirmed through analysis of the line-fitting plots of the carbon signals. Therefore, the chemical shifts of Ce metallofullerenes are expressed briefly as eq. 2, in which r represents the distance between Ce and cage carbons, θ is the angle between the \mathbf{r} vector and the C₂ axis of Ce@C_{2v}-C₈₂, and C is a common constant with a negative value for all cage carbons.

$$\delta = \delta_{\text{dia}} + \delta_{\text{fc}} + \delta_{\text{pc}} = \delta_{\text{dia}} + c_{\text{fc}}/T + c_{\text{pc}}/T^2 \quad (1)$$

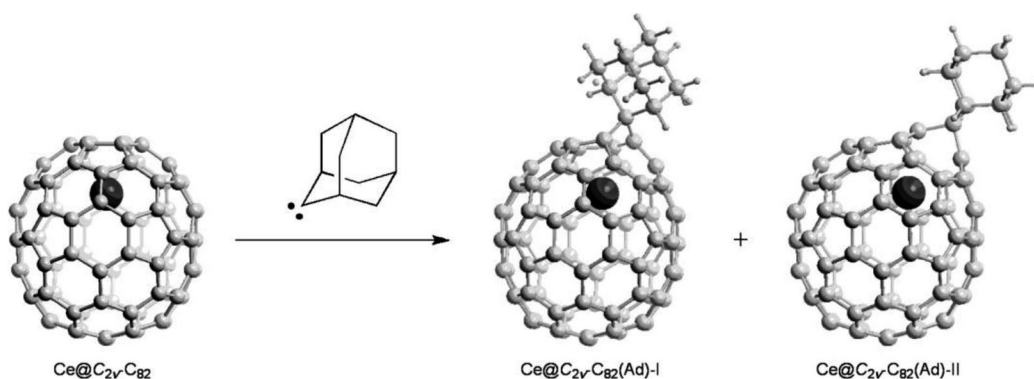
$$\delta = \delta_{\text{dia}} + c_{\text{pc}}/T^2 = \delta_{\text{dia}} + C(3 \cos^2\theta - 1)/(r^3 T^2) \quad (2)$$

It is noteworthy that c_{pc} includes geometrical information (r and θ) related to the encapsulated Ce atoms. We conducted variable-temperature (VT) ¹³C NMR measurements of Ce@C_{2v}-C₈₂ anion to obtain the experimental c_{pc} values. Use of the least-squares method revealed the distance between Ce and the center of the hexagonal ring along the C₂ axis to be 2.1–2.8 Å. This metal position corresponds to

the minimum of the electrostatic potential of $C_{2v}\text{-}C_{82}^{3-}$ [19]. This agreement is important evidence that the electrostatic metal–cage interaction plays a dominant role in determining the metal position.

Carbene adducts

Carbene addition is an efficient method to derivatize $M@C_{2v}\text{-}C_{82}$ ($M = \text{La}$ [20,21] and Gd [22]), in which adamantylidene (Ad) carbene was used for the selective derivatization. Furthermore, $\text{Ce}@C_{2v}\text{-}C_{82}$ reacts with Ad carbene regioselectively to yield only two regioisomers: C_1 symmetric $\text{Ce}@C_{2v}\text{-}C_{82}(\text{Ad})\text{-I}$ and C_s symmetric $\text{Ce}@C_{2v}\text{-}C_{82}(\text{Ad})\text{-II}$ (Scheme 1) [23]. In both cases, the C–C bonds on the addition sites were cleaved by adding the electrophilic carbenes to form the [6,6]-open structures. Electrochemical reduction of the carbene adducts enabled the ^{13}C NMR measurements of their anions to be useful for paramagnetic NMR shift analyses. Surprisingly, the observed paramagnetic NMR shifts in $\text{Ce}@C_{2v}\text{-}C_{82}(\text{Ad})\text{-I}$ and $\text{Ce}@C_{2v}\text{-}C_{82}(\text{Ad})\text{-II}$ show good agreement with the calculated values of the optimized structures based on eq. 2 despite their lower symmetries. It is noteworthy that the Ce atoms are changed slightly by the carbene addition and are located at single sites nearest the addition sites in the carbene adducts. The absorption features of the carbene adducts are almost identical to those of pristine $\text{Ce}@C_{2v}\text{-}C_{82}$. This strong similarity suggests that the carbene addition scarcely changes the π -electron system of the cage because the sp^2 -character of the carbon atoms at the addition site is retained.



Scheme 1

Molecular structure of $\text{Ce}_2@D_2(10611)\text{-}C_{72}$

The smallest Ce-containing dimetallofullerene, $\text{Ce}_2@D_2(10611)\text{-}C_{72}$, was first reported in 2001 by Dunsch and co-workers [24]. However, the structure was not determined at that time. In 2008, we synthesized substantial amounts of $\text{Ce}_2@D_2(10611)\text{-}C_{72}$ and elucidated the cage frameworks and the metal positions using NMR spectroscopy [25]. All carbon chemical shifts of $\text{Ce}_2@D_2(10611)\text{-}C_{72}$ show considerable temperature dependence originating from the f-electron spins remaining on the Ce atoms. It is noteworthy that the paramagnetic NMR shift analysis is also applicable for dimetallofullerenes. The fundamental assumption in the analysis is that the pseudocontact shifts are produced using a sum of the individual contributions from the two Ce atoms. It is particularly interesting that $\text{Ce}_2@D_2(10611)\text{-}C_{72}$ does not obey the isolated-pentagon rule (IPR). It is expected that the Ce atoms stabilize the fused pentagons of the non-IPR cage. In fact, the paramagnetic NMR shift analysis revealed that the Ce atoms face the two fused pentagons on the two poles of the $\text{Ce}_2@D_2(10611)\text{-}C_{72}$ cage. Indeed, the ^{13}C NMR signals of the fused pentagons showed drastic temperature dependence because of the strong paramagnetic effects of the facing Ce atoms. The results obtained from the paramagnetic NMR shift analysis agree well with the computational calculations (Fig. 1).

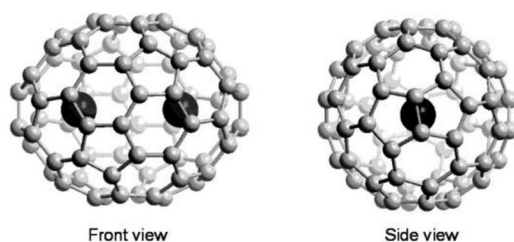


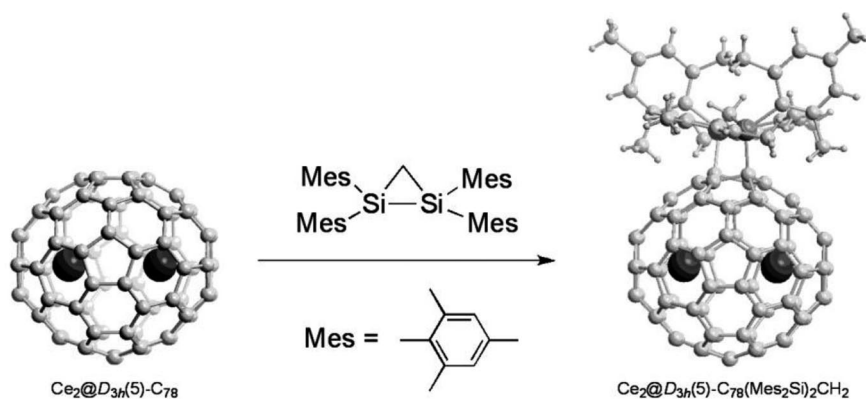
Fig. 1 Optimized structure of $\text{Ce}_2@D_2(10611)\text{-C}_{72}$.

Molecular structure of $\text{Ce}_2@D_{3h}(5)\text{-C}_{78}$

In 2008, $\text{Ce}_2@D_{3h}(5)\text{-C}_{78}$ was synthesized and isolated for the first time [26]. The ^{13}C NMR spectrum shows five lines with full intensities and three lines with half intensities, which is attributed to the $D_{3h}(5)\text{-C}_{78}$ cage structure. All carbon chemical shifts show considerable temperature dependence, as in the case of $\text{Ce}_2@D_2(10611)\text{-C}_{72}$. The paramagnetic NMR shift analysis disclosed that the Ce atoms in $\text{Ce}_2@D_{3h}(5)\text{-C}_{78}$ are localized on the C_3 axis of the ellipsoidal cage. This result agrees well with the optimized structure of $\text{La}_2@D_{3h}(5)\text{-C}_{78}$ calculated using the density functional theory (DFT) method. The absorption spectrum of $\text{Ce}_2@D_{3h}(5)\text{-C}_{78}$ shows characteristic absorptions at 644, 553, and 526 nm, which resembles that of $\text{La}_2@D_{3h}(5)\text{-C}_{78}$ [27].

Bis-silylated adduct

Bis-silylation of $\text{Ce}_2@D_{3h}(5)\text{-C}_{78}$ with 1,1,2,2-tetramesityl-1,2-disilirane proceeded smoothly at elevated temperature (80 °C) to afford the bis-silylated adduct, $\text{Ce}_2@D_{3h}(5)\text{-C}_{78}(\text{Mes}_2\text{Si})_2\text{CH}_2$ (Mes = mesityl) [26]. The absorption spectrum of the bis-silylated adduct shows an absorption maximum at 957 nm, which differs greatly from that of $\text{Ce}_2@D_{3h}(5)\text{-C}_{78}$. This large difference in the absorptions is ascribed to the fact that the electronic structure is strongly altered by the electron donation from the silyl substituent to the $D_{3h}(5)\text{-C}_{78}$ cage. This trend is in sharp contrast to the case of the Ad carbene adduct of $\text{La}_2@D_{3h}(5)\text{-C}_{78}$ [27]. The detailed structure of the bis-silylated adduct was elucidated using the single-crystal X-ray crystallographic analysis. In addition, the observed paramagnetic NMR shift analysis revealed that the Ce atoms are localized more tightly on the C_3 axis of the $D_{3h}(5)\text{-C}_{78}$ cage in the bis-silylated adduct. This finding agrees well with the X-ray structure.



Scheme 2

Molecular structure of $\text{Ce}_2@I_h\text{-C}_{80}$

The most abundant dimetallofullerene is known to be $\text{Ce}_2@I_h\text{-C}_{80}$, in which the two encaged metal atoms move freely. The presence of only two signals with a 3:1 intensity ratio in the ^{13}C NMR spectrum shows that the 3D random circulation of the two Ce atoms reduces the symmetry of the molecule to be icosahedral [28], as in the case of $\text{La}_2@I_h\text{-C}_{80}$ [29]. The two signals showed very slight temperature dependence compared to those of $\text{Ce}_2@D_2(10611)\text{-C}_{72}$ and $\text{Ce}_2@D_{3h}(5)\text{-C}_{78}$, despite the fact that two Ce atoms are contained in them. It is reasonable to consider that the 3D movement of the Ce atoms causes delocalization of the f-electron spins, which reduces the paramagnetic effects.

Bis-silylated adduct

Thermal reaction of $\text{Ce}_2@I_h\text{-C}_{80}$ with 1,1,2,2-tetramesityl-1,2-disilirane took place smoothly to afford a single isomer of the bis-silylated adduct, $\text{Ce}_2@I_h\text{-C}_{80}(\text{Mes}_2\text{Si})_2\text{CH}_2$, in which the two silicon atoms of the substituent are attached on the 1,4-position of the $I_h\text{-C}_{80}$ cage [28]. Results of the X-ray crystallographic analyses showed that the two Ce atoms are localized at two positions directing the hexagonal ring at the equator. Additionally, we observed strong temperature dependence of six quaternary carbon signals by decreasing temperatures from 303 to 253 K while taking VT- ^{13}C NMR measurements. On the other hand, the sp^3 carbon signal, which corresponds to the carbon atoms on the addition site of the cage, showed only slight temperature dependence. This observation is explainable by the fact that each Ce atom faces a hexagonal ring at the equator of the cage, as revealed in the X-ray crystal structure (Fig. 2). This report constitutes the first experimental evidence for control of the motion of encapsulated atoms inside a fullerene cage. The Ce–Ce distance of 3.829 Å in $\text{Ce}_2@I_h\text{-C}_{80}(\text{Mes}_2\text{Si})_2\text{CH}_2$ is shorter than that in $\text{Ce}_2@D_{3h}(5)\text{-C}_{78}(\text{Mes}_2\text{Si})_2\text{CH}_2$. However, the average distance of 2.521 Å between the Ce atoms and the nearest carbon atoms in $\text{Ce}_2@I_h\text{-C}_{80}(\text{Mes}_2\text{Si})_2\text{CH}_2$ differs little from that of 2.510 Å in $\text{Ce}_2@D_{3h}(5)\text{-C}_{78}(\text{Mes}_2\text{Si})_2\text{CH}_2$. Subsequently, we synthesized the corresponding bis-silylated analogs of $\text{La}_2@I_h\text{-C}_{80}$, $\text{La}_2@I_h\text{-C}_{80}(\text{Mes}_2\text{Si})_2\text{CH}_2$, and $\text{La}_2@I_h\text{-C}_{80}(\text{Dep}_2\text{Si})_2\text{CH}_2$ (Dep = 2,6-diethylphenyl) [30]. The VT- ^{139}La NMR study of $\text{La}_2@I_h\text{-C}_{80}(\text{Dep}_2\text{Si})_2\text{CH}_2$ revealed that the two metal atoms do not stand still but instead hop two-dimensionally inside the bis-silylated cage in solution. Two Ce atoms in $\text{Ce}_2@I_h\text{-C}_{80}(\text{Mes}_2\text{Si})_2\text{CH}_2$ have restricted movement as well. Therefore, we conclude that the metal atoms in bis-silylated $I_h\text{-C}_{80}$ hop two-dimensionally along the equator. This hopping movement is supported by results of computational studies that preceded the experimental observations [31]. It is expected that the electrostatic potential inside the cage was transformed by bis-silylation because of the electron donation of ca. 0.9 electron from the silyl substituent. The absorption spectrum of $\text{Ce}_2@I_h\text{-C}_{80}(\text{Mes}_2\text{Si})_2\text{CH}_2$ in a toluene solution shows an absorption maximum at 819 nm, whereas that of $\text{Ce}_2@I_h\text{-C}_{80}$ exhibits a featureless absorption. Such a large difference between the absorption spectra of

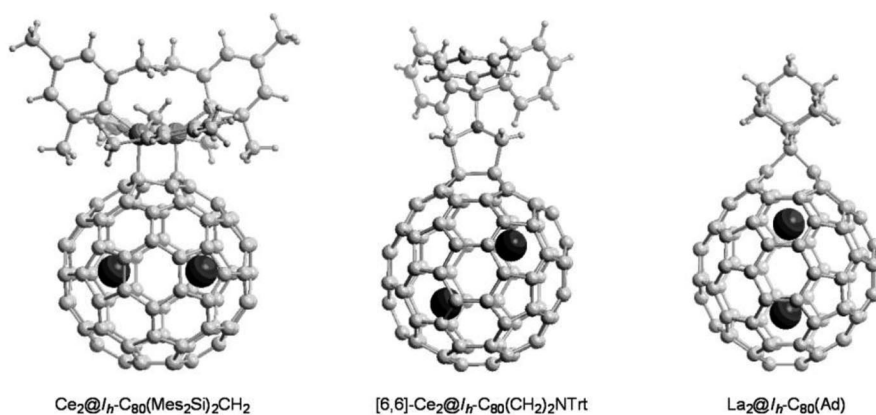


Fig. 2 X-ray structures of $\text{M}_2@I_h\text{-C}_{80}$ derivatives.

$Ce_2@I_h-C_{80}$ and the bis-silylated adduct is ascribed to the change of the electronic structure of the cage, which results from the electron donation from the silyl substituent to the cage.

Carbene adduct

To form the [6,6]-open adduct, $Ce_2@I_h-C_{80}(Ad)$, $Ce_2@I_h-C_{80}$ reacts with Ad carbene, in which the [6,6]-bond is broken by its addition [32]. We performed X-ray crystallographic analysis of the $La_2@I_h-C_{80}$ analog, $La_2@I_h-C_{80}(Ad)$, which revealed that the metal atoms are collinear with the spiro carbon of the carbene adduct, unlike the 3D random movement in $La_2@I_h-C_{80}$ (Fig. 2). It is noteworthy that the La–La distance is highly elongated to 4.031 Å. The remarkable metal–metal elongation in the carbene adduct results from the expansion of the cage's inner space caused by the bond cleavage, which reduces the electrostatic repulsion between the metal cations. This elongation engenders the regulation of metal atoms from 3D movement to the restricted behavior. In addition, the paramagnetic NMR shift analysis of $Ce_2@I_h-C_{80}(Ad)$ indicates that the Ce positions are also regulated and stand still at specific positions that are collinear with the spiro carbon of the Ad carbene at room temperature in solution, as found for $La_2@I_h-C_{80}(Ad)$. The absorption spectra of $La_2@I_h-C_{80}(Ad)$ and $Ce_2@I_h-C_{80}(Ad)$, respectively, resemble those of the pristine $La_2@I_h-C_{80}$ and $Ce_2@I_h-C_{80}$. These facts indicate that the π -electronic state of the I_h-C_{80} cage is little changed by the carbene addition because the sp^2 -character of the carbon atoms at the addition site is retained.

1,3-Dipolar cycloadducts

Exclusion of carbon dioxide from 3-trityl-5-oxazolidinone under heating in toluene generates the corresponding 1,3-dipolar reagent, which adds readily to $La_2@I_h-C_{80}$ yielding both [6,6]-closed and [5,6]-closed cycloadducts of $La_2@I_h-C_{80}(CH_2)_2NTrt$ (Trt = trityl) [33]. Similarly, the 1,3-dipolar cycloaddition of $Ce_2@I_h-C_{80}$ afforded [6,6]-closed and [5,6]-closed cycloadducts of $Ce_2@I_h-C_{80}(CH_2)_2NTrt$ [34]. The structures of [6,6]- $La_2@I_h-C_{80}(CH_2)_2NTrt$ and [6,6]- $Ce_2@I_h-C_{80}(CH_2)_2NTrt$ were elucidated unambiguously using X-ray crystallography. The metal positions in the [6,6]-closed adducts are fixed at slantwise positions on the mirror plane (Fig. 2). Regarding [6,6]- $Ce_2@I_h-C_{80}(CH_2)_2NTrt$, the metal positions obtained using the paramagnetic NMR shift analysis agree well with the X-ray structure. In contrast, the paramagnetic NMR shift analysis of [5,6]- $Ce_2@I_h-C_{80}(CH_2)_2NTrt$ exhibited that the two Ce atoms are collinear with the pyrrolidine ring. The metal positions in the [6,6]-adduct and [5,6]-adduct are explainable by the electrostatic potential maps inside the cages. This finding indicates that the metal positions are controllable by the positions of the addends' addition. The absorption spectra of [5,6]- $La_2@I_h-C_{80}(CH_2)_2NTrt$ and [5,6]- $Ce_2@I_h-C_{80}(CH_2)_2NTrt$, respectively, resemble those of the pristine $La_2@I_h-C_{80}$ and $Ce_2@I_h-C_{80}$. On the other hand, it is worth noting that a broad absorption peak centered 687 nm for [6,6]- $La_2@I_h-C_{80}(CH_2)_2NTrt$, which is not present in [5,6]- $La_2@I_h-C_{80}(CH_2)_2NTrt$. Similarly, the absorption spectrum of [6,6]- $Ce_2@I_h-C_{80}(CH_2)_2NTrt$ exhibits a broad peak at 652 nm, which is not present in [5,6]- $Ce_2@I_h-C_{80}(CH_2)_2NTrt$.

Molecular structure of $Ce_2@D_{5h}-C_{80}$

Very recently, we synthesized and characterized a second $Ce_2@C_{80}$ isomer: $Ce_2@D_{5h}-C_{80}$ [35]. The ^{13}C NMR spectrum of $Ce_2@D_{5h}-C_{80}$ shows two full-intensity lines and four half-intensity lines, which are attributed to the D_{5h} -symmetry of this molecule. It is particularly interesting that the observed c_{pc} values of the carbon signals are larger than those of $Ce_2@D_{3h}(5)-C_{78}$, in which the two Ce atoms are stationary at specific positions. The strong temperature-dependence of the carbon signals indicates that the two Ce atoms in $Ce_2@D_{5h}-C_{80}$ do not circulate three-dimensionally; instead, they move in a restricted manner. The paramagnetic NMR shift analysis together with theoretical calculations led us to conclude that the Ce atoms in $Ce_2@D_{5h}-C_{80}$ circulate two-dimensionally along a band of 10 contiguous hexagons (Fig. 3), which contrasts sharply to the 3D movement of two Ce atoms in $Ce_2@I_h-C_{80}$. In fact, the ^{13}C signals of $Ce_2@D_{5h}-C_{80}$ displays larger temperature dependence than those of $Ce_2@I_h-$

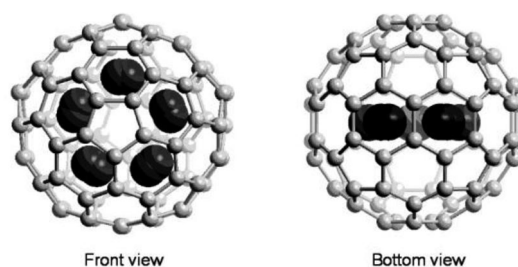


Fig. 3 Optimized structure of $\text{Ce}_2@D_{5h}\text{-C}_{80}$, in which five equivalent D_{5h} positions of Ce atoms are depicted.

C_{80} , reflecting the restricted circulation of the Ce atoms in $\text{Ce}_2@D_{5h}\text{-C}_{80}$. This finding underscores the fact that the dynamic movement of the metal atoms depends not only on the size, but also on the fullerene cage symmetry.

Electronic properties of fullerene endohedrals

Table 1 presents redox potentials of the fullerene endohedrals. The electrochemical properties of fullerene endohedrals are highly dependent on both the cage size and on the cage symmetry. Among these endohedrals, $\text{Ce}@C_{2v}\text{-C}_{82}$ shows the lowest first oxidation potential (0.08 V) and third lowest reduction potential, characterizing the lowest electrochemical potential gap. This observation is attributable to the open-shell electronic structure caused by the three-electron transfer from the Ce atom to the carbon cage. It is particularly interesting that dimetallofullerenes also have lower electrochemical potential gaps compared to C_{60} despite the closed-shell electronic structure. Theoretical calculations display that the lowest unoccupied molecular orbitals (LUMOs) of the dimetallofullerenes are localized on the two metal cations, which contrasts sharply to the case of monometallofullerenes, in which the LUMOs are distributed not only to the metal cations but also to the carbon cages. In $\text{Ce}_2@D_2(10611)\text{-C}_{72}$, two reversible reductions, one reversible oxidation, and one irreversible oxidation potential were observed. The reversibility at the first oxidation as well as the first and second reduction is consistent with the fact that the $\text{Ce}_2@D_2(10611)\text{-C}_{72}$ molecule is stable under ambient conditions, despite its non-IPR structure. In addition, $\text{Ce}_2@D_2(10611)\text{-C}_{72}$ has much lower oxidation and higher reduction potentials than $\text{Ce}_2@I_h\text{-C}_{80}$ has [28]. Indeed, the highest occupied molecular orbital (HOMO)–LUMO gap of $\text{Ce}_2@D_2(10611)\text{-C}_{72}$ is larger than those of previously reported endohedral dimetallofullerenes, such as $\text{La}_2@I_h\text{-C}_{80}$ [36]. These results are consistent with the theoretical calculations. In $\text{Ce}_2@D_{3h}(5)\text{-C}_{78}$, three reversible reductions, one reversible oxidation, and one irreversible oxidation potential were observed. The first reduction potential of $\text{Ce}_2@D_{3h}(5)\text{-C}_{78}$ is lower than that of $\text{Ce}_2@D_2(10611)\text{-C}_{72}$, indicating the higher reactivity of $\text{Ce}_2@D_{3h}(5)\text{-C}_{78}$ toward disilirane. Indeed, $\text{Ce}_2@D_{3h}(5)\text{-C}_{78}$ reacts with disilirane thermally, but $\text{Ce}_2@D_2(10611)\text{-C}_{72}$ does not. It is particularly interesting that the I_h -symmetric larger dimetallofullerene, $\text{Ce}_2@I_h\text{-C}_{80}$, has higher oxidation potentials and lower reduction potentials compared to those of the smaller dimetallofullerenes. Remarkably, $\text{Ce}_2@I_h\text{-C}_{80}$ is easier to reduce than $\text{Ce}@C_{2v}\text{-C}_{82}$. Moreover, the electrochemical reduction processes of $\text{Ce}_2@D_{5h}\text{-C}_{80}$ closely resemble those of $\text{Ce}_2@I_h\text{-C}_{80}$. On the other hand, the first oxidation potential of $\text{Ce}_2@D_{5h}\text{-C}_{80}$ is lower than that of $\text{Ce}_2@I_h\text{-C}_{80}$. In fact, $\text{Ce}_2@D_{5h}\text{-C}_{80}$ possesses the lowest HOMO–LUMO gap reported to date for fullerene endohedrals with closed-shell electronic structures.

Table 1 Redox potentials (in V vs. Fc⁺/Fc) of fullerene endohedrals^a.

Compound	ox E_3	ox E_2	ox E_1	red E_1	red E_2	red E_3
Ce@C _{2v} -C ₈₂ ^d		1.08 ^{b,c}	0.08	-0.41	-1.41	-1.53
Ce ₂ @D ₂ (10611)-C ₇₂ ^e		0.82 ^{b,c}	0.18	-0.81	-1.86	
Ce ₂ @D _{3h} (5)-C ₇₈ ^f		0.79 ^{b,c}	0.25 ^b	-0.52 ^b	-1.86 ^b	-2.23 ^b
Ce ₂ @I _h -C ₈₀ ^g		0.95	0.57	-0.39	-1.71	
Ce ₂ @D _{5h} -C ₈₀ ^h	0.86 ^b	0.66 ^b	0.20	-0.40	-1.76	-2.16
C ₆₀ ^d			1.21 ^{b,c}	-1.12	-1.50	-1.95

^aHalf-cell potentials unless otherwise stated.^bValues were obtained using differential pulse voltammetry.^cIrreversible.^dRef. [37].^eRef. [25].^fRef. [26].^gRef. [28].^hRef. [35].

It is also of interest how the electronic properties are modulated upon exohedral functionalization because the fine-tuning of the electron affinity of the fullerene endohedrals is desired for the direction of photovoltaic applications. The redox potentials of functionalized derivatives of fullerene endohedrals are presented in Table 2. The Ad carbene adducts of Ce@C_{2v}-C₈₂ showed slightly higher first-reduction potentials, but lower first-oxidation potentials than the pristine Ce@C_{2v}-C₈₂, indicating that the introduction of an Ad carbene group decreases the electron-accepting ability because of the inductive effect. Similar behavior was also apparent for the Ad carbene adduct of Ce₂@I_h-C₈₀. Indeed, the first oxidation potential of Ce₂@I_h-C₈₀(Ad) was shifted cathodically by 100 mV; the first reduction potentials were shifted cathodically by 40 mV as compared to pristine Ce₂@I_h-C₈₀. The small shifts of oxidation and reduction potentials reflect the fact that the HOMO–LUMO gap of Ce₂@I_h-C₈₀(Ad) resembles that of pristine Ce₂@I_h-C₈₀. In contrast, bis-silylation strongly affects the redox properties of fullerene endohedrals. The bis-silylated adduct of Ce₂@D_{3h}(5)-C₇₈ exhibited one irreversible and one reversible oxidation waves as well as one reversible reduction wave in the cyclic voltammogram. Compared to Ce₂@D_{3h}(5)-C₇₈, all the oxidation and reduction potentials of the bis-silylated adduct are shifted cathodically by 290 mV. This observation indicates that the D_{3h}(5)-C₇₈ cage was negatively charged to a considerable extent by bis-silylation because the silyl substituent acts as a strong electron donor. Therefore, the bis-silylation shifted the first reduction potential to more negative potentials. It is particularly interesting that the bis-silylated Ce₂@D_{3h}(5)-C₇₈ is stable at the first oxidation potential, but the quantitative retro-cycloaddition takes place at the second-oxidation potential. The first oxidation and reduction potentials of the bis-silylated Ce₂@I_h-C₈₀ were shifted cathodically, respectively, by 640 and 340 mV. It is noteworthy that the first oxidation of the bis-silylated Ce₂@I_h-C₈₀ led to removal of the silyl substituent from the carbon cage. We also investigated the redox properties of the two regioisomers of 1,3-dipolar cycloadducts of Ce₂@I_h-C₈₀. The first oxidation and reduction potentials of [6,6]-Ce₂@I_h-C₈₀(CH₂)₂NTrt cycloadduct were cathodically shifted, respectively, by 10 and 160 mV. On the other hand, the corresponding oxidation and reduction potentials of [5,6]-Ce₂@I_h-C₈₀(CH₂)₂NTrt were cathodically shifted, respectively, by 350 and 120 mV. Such a drastic difference in the redox potentials of the two regioisomers is important evidence that the respective π -electron systems of the fullerene cages in the [6,6]-cycloadduct and [5,6]-cycloadduct differ greatly. It is reasonable to infer that the different electronic properties engender the different movements of the encapsulated metal atoms in the two regioisomers.

Table 2 Redox potentials (in V vs. Fc⁺/Fc) of functionalized derivatives of fullerene endohedrals^a.

Compound	^{ox} E ₃	^{ox} E ₂	^{ox} E ₁	^{red} E ₁	^{red} E ₂	^{red} E ₃
Ce@C _{2v} -C ₈₂ ^d		1.08 ^{b,c}	0.08	-0.41	-1.41	-1.53
Ce@C _{2v} -C ₈₂ (Ad)-I ^e			0.01 ^b	-0.41 ^b	-1.36 ^b	-1.72 ^b
Ce@C _{2v} -C ₈₂ (Ad)-II ^e			0.02 ^b	-0.42 ^b	-1.35 ^b	-1.74 ^b
Ce ₂ @D _{3h} (5)-C ₇₈ ^f		0.79 ^{b,c}	0.25 ^b	-0.52 ^b	-1.86 ^b	-2.23 ^b
Ce ₂ @D _{3h} (5)-C ₇₈ (Mes ₂ Si) ₂ CH ₂ ^f		0.50 ^{b,c}	-0.04 ^b	-0.81 ^b		
Ce ₂ @I _h -C ₈₀ ^g		0.95	0.57	-0.39	-1.71	
Ce ₂ @I _h -C ₈₀ (Mes ₂ Si) ₂ CH ₂ ^g			-0.07 ^{b,c}	-0.73		
Ce ₂ @I _h -C ₈₀ (Ad) ^h		0.89 ^b	0.47	-0.43		
[6,6]-Ce ₂ @I _h -C ₈₀ (CH ₂) ₂ NTrt ⁱ		0.99 ^{b,c}	0.56 ^b	-0.55 ^b	-1.75 ^b	-2.34 ^b
[5,6]-Ce ₂ @I _h -C ₈₀ (CH ₂) ₂ NTrt ⁱ	1.02 ^{b,c}	0.62 ^b	0.22 ^b	-0.51 ^b	-1.76 ^b	-2.25 ^b

^aHalf-cell potentials unless otherwise stated.^bValues were obtained using differential pulse voltammetry.^cIrreversible.^dRef. [37].^eRef. [23].^fRef. [26].^gRef. [28].^hRef. [32].ⁱRef. [34].

CONCLUSIONS

The explanations presented herein describe the synthesis and characterization of a series of fullerene endohedrals and their derivatives. The molecular structures including the dynamic behaviors of the metal atoms were elucidated using paramagnetic NMR shift analysis together with X-ray crystallography and computational calculations. Results showed that the metal atoms' locations and movements depend drastically not only on the cage sizes and symmetries but also on the exohedral addends. Electrochemical investigations revealed that fullerene endohedrals have much lower oxidation and reduction potentials than those of hollow fullerenes. The redox properties also drastically depend on the cage sizes and symmetries. These redox properties can be modulated through exohedral chemical functionalization. The reduction potentials are dependent on the addends' electron-donating abilities and on the addition site locations. Results of these systematic studies of fullerene endohedrals will engender a deeper understanding of spherical π -electron systems.

ACKNOWLEDGMENTS

This work was supported in part by a Grant-in-Aid for Scientific Research on Innovative Areas (No. 20108001, "pi-Space"), a Grant-in-Aid for Scientific Research (A) (No. 20245006), The Next Generation Super Computing Project (Nanoscience Project), Nanotechnology Support Project, and Grants-in-Aid for Scientific Research in Priority Areas (Nos. 20036008, 20038007) from the Ministry of Education, Culture, Sports, Science, and Technology of Japan. M. Y. thanks the Japan Society for the Promotion of Science (JSPS) for the Research Fellowship for Young Chemists.

REFERENCES AND NOTES

1. H. W. Kroto, J. R. Heath, S. C. O'Brien, R. F. Curl, R. E. Smalley. *Nature* **318**, 162 (1985).
2. T. Akasaka, S. Nagase (Eds.). *Endofullerenes: A New Family of Carbon Clusters*, Kluwer, Dordrecht (2002).

3. H. Shinohara. *Rep. Prog. Phys.* **63**, 843 (2000).
4. M. Yamada, T. Akasaka, S. Nagase. *Acc. Chem. Res.* **43**, 92 (2010).
5. To designate isomers of hollow fullerenes, the carbon cages are labeled by their symmetry and the number in accordance with the Fowler–Monolopoulos spiral algorithm. Usually, a short form of numbering system is used, in which only IPR isomers are numbered. In this paper, a short form of numbering system is used for IPR isomers, as given in “An Atlas of Fullerenes”, while full numbering system is adopted for non-IPR isomers to simplify comparison of the discussion in this paper with previous literatures. See: (a) P. Fowler, D. E. Manolopoulos. *An Atlas of Fullerenes*, Clarendon Press, Oxford (1995). This two-fold numbering system is also used in a recent review written by A. A. Popov. See: (b) A. A. Popov. *J. Comput. Theor. Nanosci.* **6**, 1 (2008).
6. T. Akasaka, T. Wakahara, S. Nagase, K. Kobayashi, M. Waelchli, K. Yamamoto, M. Kondo, S. Shirakura, S. Okubo, Y. Maeda, T. Kato, M. Kako, Y. Nakadaira, R. Nagahata, X. Gao, E. Van Caemelbecke, K. M. Kadish. *J. Am. Chem. Soc.* **122**, 9316 (2000).
7. T. Akasaka, T. Wakahara, S. Nagase, K. Kobayashi, M. Waelchli, K. Yamamoto, M. Kondo, S. Shirakura, Y. Maeda, T. Kato, M. Kako, Y. Nakadaira, X. Gao, E. Van Caemelbecke, K. M. Kadish. *J. Phys. Chem. B* **105**, 2971 (2001).
8. T. Wakahara, J. Kobayashi, M. Yamada, Y. Maeda, T. Tsuchiya, M. Okamura, T. Akasaka, M. Waelchli, K. Kobayashi, S. Nagase, T. Kato, M. Kako, K. Yamamoto, K. M. Kadish. *J. Am. Chem. Soc.* **126**, 4883 (2004).
9. T. Wakahara, S. Okubo, M. Kondo, Y. Maeda, T. Akasaka, M. Waelchli, M. Kako, K. Kobayashi, S. Nagase, T. Kato, K. Yamamoto, X. Gao, E. Van Caemelbecke, K. M. Kadish. *Chem. Phys. Lett.* **360**, 235 (2002).
10. L. Feng, T. Wakahara, T. Tsuchiya, Y. Maeda, Y. Lian, T. Akasaka, N. Mizorogi, K. Kobayashi, S. Nagase, K. M. Kadish. *Chem. Phys. Lett.* **405**, 274 (2005).
11. E. Nishibori, K. Iwata, M. Sakata, M. Takata, H. Tanaka, H. Kato, H. Shinohara. *Phys. Rev. B* **69**, 113412 (2004).
12. L. Senapati, J. Schrier, K. B. Whaley. *Nano Lett.* **4**, 2073 (2004).
13. L. Senapati, J. Schrier, K. B. Whaley. *Nano Lett.* **5**, 2341 (2005).
14. N. Mizorogi, S. Nagase. *Chem. Phys. Lett.* **431**, 110 (2006).
15. L. Liu, B. Gao, W. Chu, D. Chen, T. Hu, C. Wang, L. Dunsch, A. Marcelli, Y. Luo, Z. Wu. *Chem. Commun.* 474 (2008).
16. M. Yamada, T. Wakahara, Y. Lian, T. Tsuchiya, T. Akasaka, M. Waelchli, N. Mizorogi, S. Nagase, K. M. Kadish. *J. Am. Chem. Soc.* **128**, 1400 (2006).
17. B. Bleaney. *J. Magn. Reson.* **8**, 91 (1972).
18. T. Tsuchiya, T. Wakahara, Y. Maeda, T. Akasaka, M. Waelchli, T. Kato, H. Okubo, N. Mizorogi, K. Kobayashi, S. Nagase. *Angew. Chem., Int. Ed.* **44**, 3282 (2005).
19. K. Kobayashi, S. Nagase. *Chem. Phys. Lett.* **282**, 325 (1998).
20. Y. Maeda, Y. Matsunaga, T. Wakahara, S. Takahashi, T. Tsuchiya, M. O. Ishitsuka, T. Hasegawa, T. Akasaka, M. T. H. Liu, K. Kokura, E. Horn, K. Yoza, T. Kato, S. Okubo, K. Kobayashi, S. Nagase, K. Yamamoto. *J. Am. Chem. Soc.* **126**, 6858 (2004).
21. Y. Matsunaga, Y. Maeda, T. Wakahara, T. Tsuchiya, M. O. Ishitsuka, T. Akasaka, N. Mizorogi, K. Kobayashi, S. Nagase, K. M. Kadish. *ITE Lett.* **7**, 43 (2006).
22. T. Akasaka, T. Kono, Y. Takematsu, H. Nikawa, T. Nakahodo, T. Wakahara, M. O. Ishitsuka, T. Tsuchiya, Y. Maeda, M. T. H. Liu, K. Yoza, T. Kato, K. Yamamoto, N. Mizorogi, Z. Slanina, S. Nagase. *J. Am. Chem. Soc.* **130**, 12840 (2008).
23. Y. Takano, M. Aoyagi, M. Yamada, H. Nikawa, Z. Slanina, N. Mizorogi, M. O. Ishitsuka, T. Tsuchiya, Y. Maeda, T. Akasaka, T. Kato, S. Nagase. *J. Am. Chem. Soc.* **131**, 9340 (2009).
24. L. Dunsch, A. Bartl, P. Georgi, P. Kuran. *Synth. Met.* **121**, 1113 (2001).
25. M. Yamada, T. Wakahara, T. Tsuchiya, Y. Maeda, T. Akasaka, N. Mizorogi, S. Nagase. *J. Phys. Chem. A* **112**, 7627 (2008).

26. M. Yamada, T. Wakahara, T. Tsuchiya, Y. Maeda, M. Kako, T. Akasaka, K. Yoza, E. Horn, N. Mizorogi, S. Nagase. *Chem. Commun.* 558 (2008).
27. B. Cao, T. Wakahara, T. Tsuchiya, M. Kondo, Y. Maeda, G. M. A. Rahman, T. Akasaka, K. Kobayashi, S. Nagase, K. Yamamoto. *J. Am. Chem. Soc.* **126**, 9164 (2004).
28. M. Yamada, T. Nakahodo, T. Wakahara, T. Tsuchiya, Y. Maeda, T. Akasaka, M. Kako, K. Yoza, E. Horn, N. Mizorogi, K. Kobayashi, S. Nagase. *J. Am. Chem. Soc.* **127**, 14570 (2005).
29. T. Akasaka, S. Nagase, K. Kobayashi, M. Waelchli, K. Yamamoto, H. Funasaka, M. Kako, T. Hoshino, T. Erata. *Angew. Chem., Int. Ed. Engl.* **36**, 1643 (1997).
30. T. Wakahara, M. Yamada, S. Takahashi, T. Nakahodo, T. Tsuchiya, Y. Maeda, T. Akasaka, M. Kako, K. Yoza, E. Horn, N. Mizorogi, S. Nagase. *Chem. Commun.* 2680 (2007).
31. K. Kobayashi, S. Nagase, Y. Maeda, T. Wakahara, T. Akasaka. *Chem. Phys. Lett.* **374**, 562 (2003).
32. M. Yamada, C. Someya, T. Wakahara, T. Tsuchiya, Y. Maeda, T. Akasaka, K. Yoza, E. Horn, M. T. H. Liu, N. Mizorogi, S. Nagase. *J. Am. Chem. Soc.* **130**, 1171 (2008).
33. M. Yamada, T. Wakahara, T. Nakahodo, T. Tsuchiya, Y. Maeda, T. Akasaka, K. Yoza, E. Horn, N. Mizorogi, S. Nagase. *J. Am. Chem. Soc.* **128**, 1402 (2006).
34. M. Yamada, M. Okamura, S. Sato, C. I. Someya, N. Mizorogi, T. Tsuchiya, T. Akasaka, T. Kato, S. Nagase. *Chem.—Eur. J.* **15**, 10533 (2009).
35. M. Yamada, N. Mizorogi, T. Tsuchiya, T. Akasaka, S. Nagase. *Chem.—Eur. J.* **15**, 9486 (2009).
36. T. Suzuki, Y. Maruyama, T. Kato, K. Kikuchi, Y. Nakao, Y. Achiba, K. Kobayashi, S. Nagase. *Angew. Chem., Int. Ed.* **34**, 1094 (1995).
37. T. Suzuki, K. Kikuchi, F. Oguri, Y. Nakao, S. Suzuki, Y. Achiba, K. Yamamoto, H. Funasaka, T. Takahashi. *Tetrahedron* **52**, 4973 (1996).